THE JOURNAL OF PHYSICAL CHEMISTRY B

Article

pubs.acs.org/JPCB

Transferable Force Field for Carboxylate Esters: Application to Fatty Acid Methylic Ester Phase Equilibria Prediction

Nicolas Ferrando,[†,*] Véronique Lachet,[†] and Anne Boutin[‡]

[†]IFP Energies nouvelles, 1 et 4 avenue de Bois-Préau, 92852 Rueil-Malmaison, France

[‡]Ecole Normale Supérieure, Département de Chimie, UMR 8640, CNRS-ENS-UPMC, 24 rue Lhomond, 75005 Paris, France

Supporting Information

ABSTRACT: In this work, a new transferable united-atoms force field for carboxylate esters is proposed. All Lennard-Jones parameters are reused from previous parametrizations of the AUA4 force field, and only a unique set of partial electrostatic charges is introduced for the ester chemical function. Various short alkyl-chain esters (methyl acetate, ethyl acetate, methyl propionate, ethyl propionate) and two fatty acid methylic esters (methyl oleate and methyl palmitate) are studied. Using this new force field in Monte Carlo simulations, we show that various pure compound properties are accurately predicted: saturated liquid densities, vapor pressures, vaporization enthalpies, critical properties, liquid−vapor surface tensions. Furthermore, a good accuracy is also obtained in the prediction of binary mixture pressure−composition diagrams, without introducing empirical binary interaction parameters. This highlights the transferability of the proposed force field and gives the opportunity to simulate mixtures of industrial interest: a demonstration is performed through the simulation of the methyl oleate + methanol mixture involved in the purification sections of biodiesel production processes.

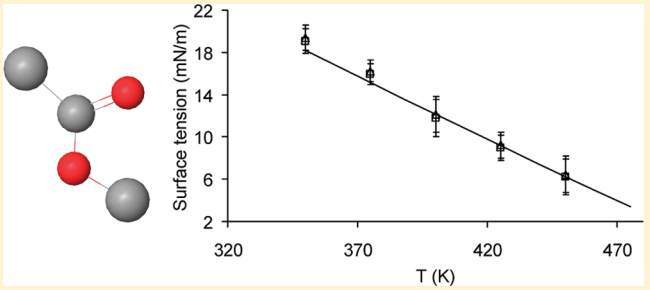

1. INTRODUCTION

The prediction of thermophysical property of systems involving esters is of primary importance in many industrial applications, e.g., the food chemistry,[1] pharmaceutics,[2] and also in the oil and gas industry.[3] For example, the knowledge of fatty acid methylic ester (FAME) properties is nowadays of great interest in biofuel synthesis since such molecules can be used both as a diesel alternative and as a diesel blending component.[4−7] FAMEs are produced from vegetable oils through a transesterification reaction of triglycerides with methanol. Vegetable oils may be of different biological origins (e.g., rapeseed oil is predominant in Europe, soybean oil in North and South America, and palm oil in South East Asia). Methyl oleate ($C_{19}H_{36}O_2$) and methyl palmitate ($C_{17}H_{37}O_2$) are among the most produced FAMEs with such techniques[8] (see a 2D view of these molecules in Figure S.1 in the Supporting Information). To design these industrial processes and to propose adequate biodiesel formulations, accurate models are required to predict phase equilibrium of pure esters and mixtures involving these chemical species.

For many years, transferable united-atoms force fields have been developed to make molecular simulation an efficient tool to predict thermodynamic data and phase equilibrium of a large number of pure compounds and mixtures for industrial purposes.[9−11] A first united-atoms force field for methyl acetate was proposed by Briggs et al.[12] based on previous parametrizations of the OPLS-UA force field for ethers[13] and amides.[14] Only liquid-phase properties of this molecule at room temperature have been studied, making the transferability of this model questionable. Sum et al.[15] have proposed an extension of the NERD united-atoms force field[16] to esters to predict the liquid-phase structure of triglycerides. This model, which was parametrized from methyl acetate properties, was not extended to phase equilibrium calculations for other esters. Finally, Kamath et al.[17] reused previous parametrizations of the TraPPE-UA force field[18−21] to propose a transferable united-atoms model for esters. Phase equilibria of various pure linear esters are accurately predicted, but mixtures often exhibit an overestimation of bubble pressures. The transferability of the TraPPE-UA force field was also exploited by Maerzke et al.[22] to successfully predict properties of acrylate and methacrylate monomers. In this work, we propose an extension of the transferable AUA4 force field to esters. This force field has been specially developed to predict phase equilibria of pure compounds and mixtures involving linear alkanes,[23] branched and cyclic alkanes,[24,25] olefins,[26] benzene,[27,28] alkyl-benzene,[29,30] polyaromatic hydrocarbons,[31,32] sulfur compounds,[33,34] alcohols,[35] ketones,[36] aldehydes,[36] ethers,[37] and amines.[38] In the same manner as the OPLS-UA and TraPPE-UA models, all Lennard-Jones parameters are reused from previous parametrizations of this force field, and only a unique set of partial electrostatic charges is specifically determined. To

Received: December 14, 2011
Revised: February 20, 2012
Published: February 27, 2012

   dx.doi.org/10.1021/jp212060u | J. Phys. Chem. B 2012, 116, 3239−3248

highlight the transferability of the proposed force field, short alkyl-chain esters and two FAMEs (methyl oleate and methyl palmitate) are studied. Pure compounds and binary mixtures are considered. In addition to classical saturated bulk-phase properties, liquid−vapor surface tensions of methyl acetate are also calculated using this new force field.

This paper is organized as follows: the proposed force field and simulation methods are described in Sections 2 and 3, respectively. Section 4 deals with pure compounds and binary mixture simulation results. Finally, Section 5 gives our conclusions.

2. FORCE FIELD DEVELOPMENT

2.1. Intermolecular Energy. The dispersive−repulsive intermolecular interactions between two force centers i and j are described through a 12-6 Lennard-Jones (LJ) potential

$$U_{ij}^{\mathrm{LJ}} = 4\varepsilon_{ij}\left[\left(\frac{\sigma_{ij}}{r_{ij}}\right)^{12} - \left(\frac{\sigma_{ij}}{r_{ij}}\right)^{6}\right] \tag{1}$$

where r_{ij}, ε_{ij}, and σ_{ij} are the distance, the LJ well depth, and the LJ size, respectively.

Cross Lennard-Jones parameters are obtained using Lorentz−Berthelot combining rules

$$\varepsilon_{ij} = \sqrt{\varepsilon_{ii}\varepsilon_{jj}} \tag{2}$$

$$\sigma_{ij} = \frac{1}{2}(\sigma_{ii} + \sigma_{jj}) \tag{3}$$

For all the force centers involved in the carboxylate esters which were studied, the Lennard-Jones parameters are reused from previous parametrizations of the AUA4 force field. Hence, we take advantage of the transferability feature of this force field, which allows us to avoid the introduction of new groups and parameters. In the AUA model, the Lennard-Jones center is not located on the atomic nucleus of the group, but slightly shifted by a distance δ (AUA displacement) to implicitly take into account the presence of its bonded hydrogen atoms. This parameter is also directly transferred from previous parametrizations. Therefore, methyl and methylene parameters are taken from *n*-alkanes,[23] carbonyl oxygen and carbonyl carbon from ketones,[36] and ether oxygen from ethers,[37] as illustrated in the Supporting Information (Figure S.2).

The electrostatic interaction between two partial electrostatic charges i and j is modeled by the Coulomb potential

$$U_{ij}^{\mathrm{elec}} = \frac{q_i q_j}{4\pi\varepsilon_0 r_{ij}} \tag{4}$$

where r_{ij} is the distance between charges i and j, q_i the magnitude of charge i, and ε_0 the vacuum permittivity. The use of a unique set of electrostatic charges for all the esters studied here is justified as long as the molecules have a similar dipole moment. As illustrated in Figure S.3 in the Supporting Information, the experimental gas-phase dipole moment[39] of various esters does not significantly vary with the alkyl chain length. For the esters being studied, the maximum deviation between experimental moments is less than 7%, and we assume this deviation to be sufficiently low for us to be able to directly transfer the electrostatic charges from one ester molecule to another. Moreover, it is well-known that the dipole moment of a polarizable molecule significantly differs between the gas phase and the liquid phase, and it is widely admitted that molecular models yield better results for phase equilibria prediction when the liquid-phase dipole moment is reproduced.[40] To determine the magnitude of the electrostatic charges, we adopt a procedure similar to that proposed by Eckl et al.:[41,42] an ab initio calculation is performed by placing a molecule in a dielectric medium whose dielectric constant is equal to that of the neat liquid of the given molecule, and the magnitude of the partial charges is adjusted to reproduce the obtained dipole moment $\mu_{\mathrm{liquid}}^{\mathrm{ab\ initio}}$. Hence, it consists of minimizing the following F function by adjusting the magnitude of the charges q_i

$$F = \left\| \sum_{j=i}^{N} q_i \mathbf{r}_i \right\| - \mu_{\mathrm{liquid}}^{\mathrm{ab\ initio}} \tag{5}$$

where N is the number of electrostatic charges and $\mathbf{r}_i$ the ith charge position given by the intramolecular parameters of the AUA4 force field.

To determine $\mu_{\mathrm{liquid}}^{\mathrm{ab\ initio}}$, preliminary ab initio calculations using the Jaguar software (v.7.0, Schrödinger LLC, 2007) and various levels of theory have shown that the B3LYP/6-311G(d,p) method gives an accurate prediction of experimental gas-phase dipole moments (see Figure S.4 in the Supporting Information). Hence, this level of theory is used for the calculation in the dielectric medium. The calculation is performed with a molecule of ethyl propionate, since its gas-phase dipole moment (1.75 D) is close to the average value for all esters studied here. The resulting liquid-phase dipole moment is 2.35 D, which corresponds to an increase of 35% compared to the experimental gas-phase dipole moment. Such an increase is comparable to that observed for other oxygenated compounds such as alcohols[35,43] or ethers.[37] As for previous united atoms force fields (OPLS-UA,[12] TraPPE-UA,[17] NERD[15]), we adopt a distribution of five electrostatic charges localized on the central atom of the functional group. Consequently, the solution of eq 5 is not unique. In a first attempt, the charges directly given by the ab initio calculation (least-squares fit of the ab initio electrostatic potential of the molecule) were selected. However, this choice leads to poor predictions for density and vapor pressure of the various esters. Thus, using a trial and error procedure and with a constraint to keep the dipole moment equal to 2.35 D, charges are tuned to obtain better predictions of saturated liquid densities and vapor pressures of methyl acetate and ethyl acetate. The resulting electrostatic charges are reported in Table 1.

2.2. Intramolecular Energy. All the bonded parameters involved in the intramolecular energy calculation are given in Table 2. In the proposed force field, all bond lengths are kept

Table 1. Nonbonded Parameters for Groups Involved in the Molecules Studied

group	ε (K)	σ (Å)	δ (Å)	q (e)
CH_3 ($-C_{ester}$)	120.15	3.607	0.216	−0.089
CH_2 ($-C_{ester}$)	86.29	3.461	0.384	−0.089
CH_3 ($-O-$)	120.15	3.607	0.216	+0.319
CH_2 ($-O-$)	86.29	3.461	0.384	+0.319
CH (=CH)	90.60	3.320	0.414	0
C (=O)	61.90	3.020	0	+0.484
O (=C)	96.51	2.981	0	−0.377
O ($-CH_x$)	59.69	2.991	0	−0.337

dx.doi.org/10.1021/jp212060u | J. Phys. Chem. B 2012, 116, 3239−3248

Table 2. Bonded Parameters for Groups Involved in the Molecules Studied

bond length		r_0 (Å)		ref
$CH_x–CH_y$		1.535		23
CH═CH		1.331		26
$CH_x–C(=O)$		1.522		36
C(═O)		1.229		36
O–C(═O)		1.430		37
$O–CH_x$		1.430		37
bend	θ_0 (deg)	k_{bend} (K)		ref
$CH_x–CH_2–CH_y$	114.0	74900		23
$CH_x–CH_2–C(=O)$	114.0	74900		36
$CH_x–CH=CH$	124.0	rigid		26
$CH_x–C(=O)=O$	120.4	105822		36
$CH_x–C(=O)–O$	119.2	105822		36
O(═C)═C–O	120.4	105822		36
C(═O)–O–CH_x	112.0	69000		37
O–CH_2–CH_x	109.47	59800		37
torsion		a_i (K)		ref
$CH_x–CH_2–CH_2–CH_y$, $CH_x–CH_2–CH_2–C(=O)$		a_0 = 1001.35	a_1 = 2129.52	23
		a_2 = −303.06	a_3 = −3612.27	
		a_4 = 2226.71	a_5 = 1965.93	
		a_6 = −4489.34	a_7 = −1736.22	
		a_8 = 2817.37		
$CH_x–CH_2–C(=O)=O$		a_0 = 198.39	a_1 = 1434.30	36
		a_2 = 482.36	a_3 = −4254.39	
		a_4 = −2010.11	a_5 = 5128.05	
		a_6 = 2214.12	a_7 = −2389.21	
		a_8 = −801.10		
$CH_x–CH_2–C(=O)–O$		a_0 = 373.05	a_1 = 919.04	36
		a_2 = 268.15	a_3 = −1737.21	
		$a_{4–8}$ = 0		
$CH_x–O–C(=O)=O$		a_0 = 6486.6	a_1 = 1733.8	17
		a_2 = −4118.0	a_3 = 613.6	
		$a_{4–8}$ = 0		
$CH_x–O–C(=O)–CH_x$		a_0 = 6551.3	a_1 = −1566.1	17
		a_2 = −4196.0	a_3 = −789.2	
		$a_{4–8}$ = 0		
$CH_x–CH_2–O–C(=O)$		a_0 = 956.05	a_1 = 949.25	37
		a_2 = 327.5	a_3 = −2232.8	
		$a_{4–8}$ = 0		
$CH_x–CH_y–CH=CH$		a_0 = 272.37	a_1 = −938.12	26
		a_2 = 220.73	a_3 = 1135.06	
		$a_{4–8}$ = 0		
$CH_x–CH=CH–CH_y$		rigid		26

fixed. The $C(sp^2)–O(–CH_x)$ bond length is assumed to be equal to the $CH_x–O(–CH_x)$ bond length found in ethers.[37] Other bond lengths are taken from the AUA4 force field. Atoms separated by two bonds interact via a harmonic bending potential

$$\frac{U_{bend}}{k_B} = \frac{1}{2}k_{bend}(\cos\theta - \cos\theta_0)^2 \quad (6)$$

where k_B is the Boltzmann constant, k_{bend} the bending constant, θ and θ_0 the bending angle and the equilibrium bending angle, respectively. We assume that the $CH_x–C(sp^2)–O$ and O═$C(sp^2)–O$ bending parameters are identical to those found in ketones for the $CH_x–C(sp^2)–CH_x$ and O═$C(sp^2)–CH_x$ angles, respectively.[36] All other bending parameters are taken from the AUA4 force field. For atoms separated by three bonds, a torsion potential of the following form is used

$$\frac{U_{tors}}{k_B} = \sum_{n=0}^{8} a_n(\cos(\varphi + \pi))^n \quad (7)$$

where φ is the dihedral angle and a_i the ith torsion parameter. The $CH_x–O–C(sp^2)–CH_x$ and $CH_x–O–C(sp^2)$═O torsion parameters are taken from the TraPPE-UA force field.[17] It is worth noting that the equation used in reference 17 (see eq 8 below) to describe the torsion potential is different from eq 7

$$\frac{U_{tors}}{k_B} = c_0 + c_1[1 + \cos(\varphi)] + c_2[1 - \cos(2\varphi)] + c_3[1 + \cos(3\varphi)] \quad (8)$$

dx.doi.org/10.1021/jp212060u | J. Phys. Chem. B 2012, 116, 3239–3248

However, trigonometric transformations give a rigorous equivalence between parameters a_i of eq 7 and parameters c_i of eq 8

$$a_0 = c_0 + c_1 + 2c_2 + c_3$$
$$a_1 = -(c_1 - 3c_3)$$
$$a_2 = -2c_2$$
$$a_3 = -4c_3 \quad (9)$$

All other torsions are taken from the AUA4 force field. The $CH_x-CH_2-C(=O)-O$ torsion is assumed to be the same as the $CH_x-CH_2-C(=O)-CH_x$ torsion encountered in ketones.[36]

Finally, a 12-6 Lennard-Jones potential is used to calculate the repulsive−dispersive intramolecular energy between two force centers separated by more than three bonds with parameters identical to those used for intermolecular interactions.

3. SIMULATION METHODS

3.1. Phase Equilibria. All the bulk liquid/vapor equilibrium simulations of pure compounds were carried out in the NVT Gibbs Ensemble.[44,45] In this ensemble, the two phases in equilibrium are introduced in two separate boxes without an explicit interface. When employed to study pure component equilibria, this ensemble is applied at constant total volume of the two phases to respect the phase rule. The temperature and the total number of molecules are also held at a constant value. A total number of 300 molecules was used for each system, except for methyl oleate and methyl palmitate for which 60 molecules were used. By simulating double-size systems (120 molecules) for methyl oleate and methyl palmitate at 600 K, finite-size effects have been estimated to be around 0.5% for liquid density, 2.7% for vapor pressure, and 0.6% for vaporization enthalpy. These values are within the statistical uncertainties (see Table S.2. in the Supporting Information). The simulation runs lasted for 50 million steps (involving an equilibration run of 25 million steps), one step corresponding to a single Monte Carlo (MC) move. In the case of Lennard-Jones interactions, a spherical cutoff equal to half of the simulation box was used, and a classical tail correction was employed to account for interactions beyond this cutoff distance.[46] For long-range electrostatic energy, the Ewald summation technique was used, with a number of reciprocal vectors k equal to 7 in all three space directions and a Gaussian width α^{red} equal to 2 in reduced units. This reduced parameter is related to the α parameter by

$$\alpha = \alpha^{red}\pi/L \quad (10)$$

where L is the simulation box length.

The different Monte Carlo moves and corresponding attempt probabilities used during the simulations depend on the molecule being studied and are summarized in the Supporting Information (Table S.1). Note that the regrowth move is performed using the configurational bias[47] and the transfer move with preinsertion and configurational biases.[48] The amplitude of translations, rigid rotations, and volume changes was adjusted during the simulation to achieve an acceptance ratio of 40% for these moves. For methyl oleate and methyl palmitate, a higher attempt probability is imposed for the transfer move since the acceptance ratio of this move is very low (0.1% at low reduced temperatures to 0.5% at high reduced temperatures). Vapor pressure is calculated using the Virial equation in the vapor phase and the molar vaporization enthalpy h^{vap} with the following relationship

$$h^{vap} = N_a\left(\frac{\langle U^{vap}\rangle}{\langle N^{vap}\rangle} - \frac{\langle U^{liq}\rangle}{\langle N^{liq}\rangle} + P^{vap}\left(\frac{\langle V^{vap}\rangle}{\langle N^{vap}\rangle} - \frac{\langle V^{liq}\rangle}{\langle N^{liq}\rangle}\right)\right) \quad (11)$$

where N_a is the Avogadro number, P^{vap} the pressure calculated in the vapor phase, and $\langle U^i\rangle$, $\langle N^i\rangle$, and $\langle V^i\rangle$ the average potential energy, total number of molecules, and volume of phase i, respectively.

For methyl oletate and methyl palmitate, simulations in the Gibbs Ensemble at 500 K (reduced temperature close to 0.65) lead to a very low number of molecules in the vapor phase, making sampling questionable. A solution would consist of increasing the total number of molecules, but it would drastically increase the computation time. Consequently, simulations at 500 K are carried out in the NPT ensemble (with a pressure of 0.1 MPa), and saturation pressure is calculated using a second-order thermodynamic integration[11]

$$\ln P_{sat}^{(n+1)} = \ln P_{sat}^{(n-1)} - \frac{h_{vap}^{(n)}}{R}(1/T^{(n+1)} - 1/T^{(n-1)}) \quad (12)$$

In this ensemble, the vaporization enthalpy can be approximated using

$$h^{vap} = -u_{inter}^{liq} + RT$$

where u_{inter}^{liq} stands for the intermolecular energy of the liquid phase. This equation assumes an ideal vapor ($u_{inter}^{vap} = 0$ and $Pv^{vap} = RT$), an equality between intramolecular molar energy between liquid and vapor phases, and a negligible liquid molar volume compared to the vapor molar volume.

The critical properties T_C and ρ_C of pure compounds were estimated by a least-squares fit of the law of rectilinear diameters

$$\frac{\rho_l + \rho_v}{2} = \rho_C + A(T - T_C) \quad (13)$$

where ρ_l and ρ_v are the density of the liquid and vapor phases, respectively, T the temperature, and A an adjustable parameter, and the critical scaling relation

$$\rho_l - \rho_v = B(T - T_C)^{\beta} \quad (14)$$

where B is another adjustable parameter and β the universal exponent, equal to 0.325.[47] This procedure works well for nonpolar molecules, but it has also been successfully used for the prediction of the critical properties of various oxygenated compounds such as alcohols, ketones, aldehydes, and ethers.[35−37] Finally, the normal boiling temperatures of the pure compounds were determined using the Clausius−Clapeyron equation.

For the binary mixtures studied in this work, simulations are performed in the bubble point pseudoensemble using the so-called hybrid method.[49,50] This methodology has already been successfully applied for nonpolar and polar mixtures with good efficiency.[36,37,50,51] The liquid-phase composition is kept fixed

during the simulation, while equilibrium pressure and vapor composition fluctuate during the simulation. In the hybrid method, a first simulation in the bubble point pseudoensemble (BPMC) is carried out, and then the results obtained are used to initialize a simulation in the isotherm-isochore Gibbs Ensemble (GE-NVT) with the main goal of reducing the statistical uncertainty in the pressure calculation. Both BPMC and GE-NVT simulations lasted for 50 to 100 million MC steps, including an equilibrium run of 30 million steps. The initial number of molecules in the liquid phase was 400, except for the methyl oleate + methanol mixture for which this quantity was fixed to 200. All other simulation parameters are similar to those previously described for pure component systems.

3.2. Surface Tension. To check the accuracy of the force field developed here to predict interfacial properties, the surface tension γ of methyl acetate was calculated. The simulations were carried out in the NVT ensemble in a rectangular parallelepiped box. We have considered a system with two planar liquid−vapor surfaces lying in the x,y plane, the z-axis being the direction normal to the surface (see Figure S.6 in the Supporting Information). As the geometry of the system shows a heterogeneity along the axis normal to the interface (z-axis), we calculated the long-range correction to the repulsion−dispersion energy as a function of z_k by splitting the cell into slabs. The total long-range correction energy U_{LRC} was then calculated by summing up all the local contributions of each slab. The U_{LRC} term was then added in the total energy of the system to be used in the Metropolis scheme. Tail corrections to the surface tension were also accounted for using the expressions given by Biscay et al.[52] More detailed descriptions of these models and long-range corrections can be found elsewhere.[53−59]

Two different methods have been used to calculate surface tensions. The first one is the Irving−Kirkwood (IK) method[60] based on the mechanical definition of the surface tension. The second method used is the Test-Area (TA) method,[61] based upon a thermodynamic route and expressing the surface tension as a change in the free energy F for a change in the surface area. Note that both methods have been successfully applied with the AUA4 force field to calculate surface tensions of various hydrocarbons[62,63] and oxygenated compounds.[37,64]

The initial configuration of the system was prepared from equilibrated bulk liquid and bulk vapor phases, the liquid phase (containing 700 molecules) being surrounded by two vapor phases (containing 10 molecules each) along the z direction. The L_x and L_y dimensions of the resulting simulation box were fixed to 40 Å, and the L_z dimension varied from 200 to 320 Å according to the temperature. The Ewald sum technique was used to calculate the electrostatic energy, with a number of reciprocal vectors equal to 8 along the x and y axis and equal to $(8{\cdot}L_z)/L_x$ along the z axis. The Monte Carlo moves and attempt probabilities used during the simulations are: translation (33.5%), rigid rotation (33.5%), and configurational-bias regrowth (33%). A typical simulation consists of an equilibration run followed by a production run of 200 million Monte Carlo steps each.

4. RESULTS

4.1.1. Pure Compounds. *Phase Equilibria.* Figures 1, 2, and 3 show experimental[39,65] and calculated saturated liquid densities, vapor pressures, and vaporization enthalpies for methyl acetate, ethyl acetate, methyl propionate, ethyl

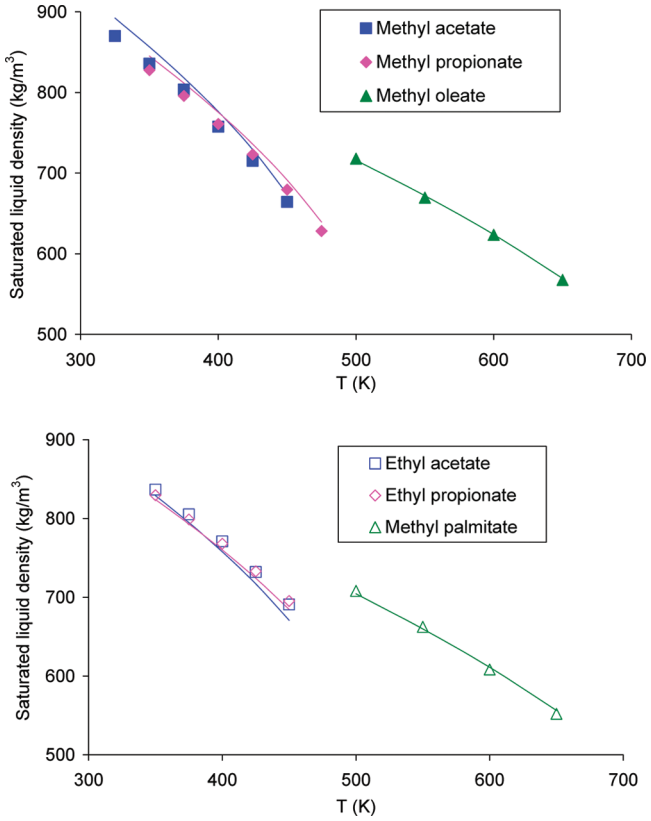

Figure 1. Experimental (lines) and calculated (symbols) saturated liquid densities of esters.

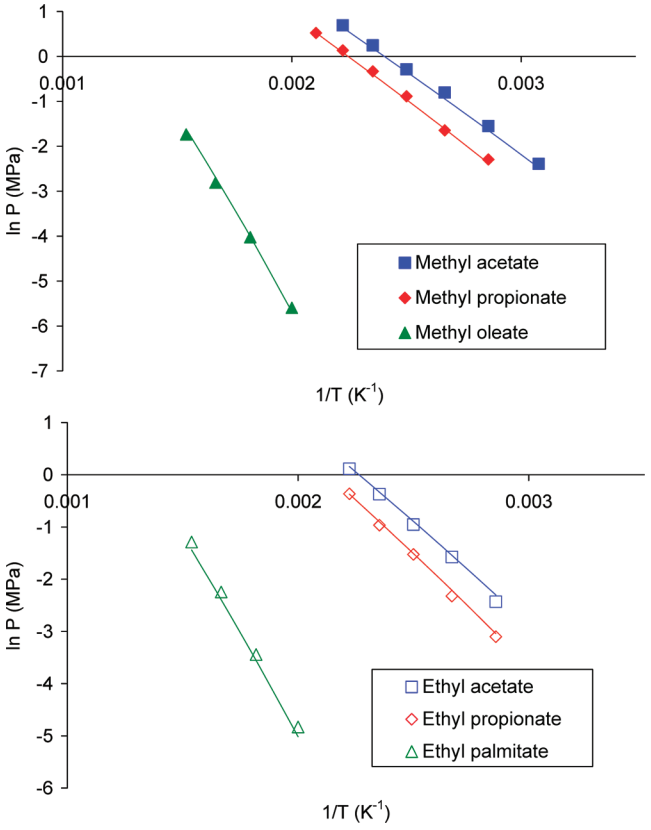

Figure 2. Experimental (lines) and calculated (symbols) vapor pressures of esters.

dx.doi.org/10.1021/jp212060u | J. Phys. Chem. B 2012, 116, 3239−3248

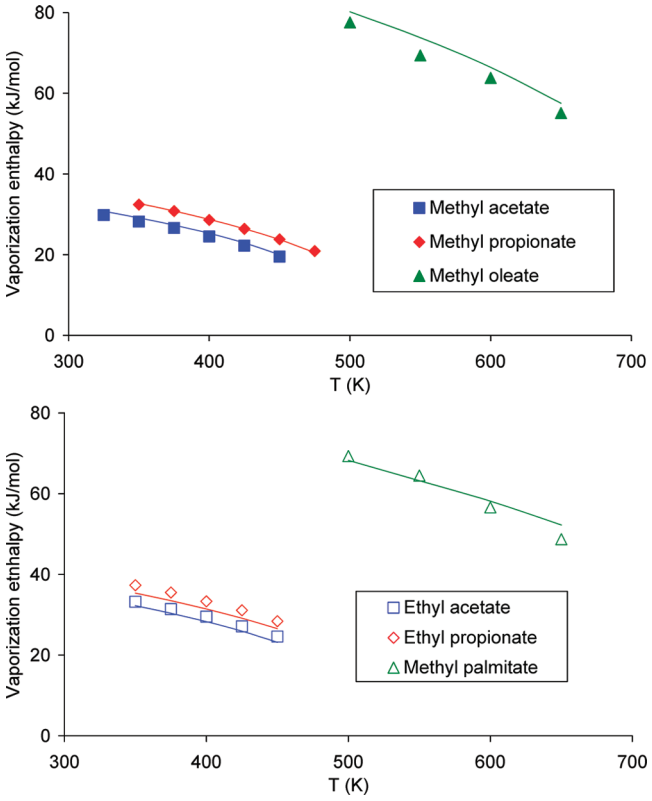

Figure 3. Experimental (lines) and calculated (symbols) vaporization enthalpies of esters.

propionate, methyl oleate, and methyl palmitate. Numerical values are reported in the Supporting Information (Table S.2). A plot of the deviation between simulation and experiments as a function of reduced temperature is shown in Figure 4 for each molecule being studied. Saturated liquid densities are accurately predicted with relative deviations ranging from −2.5 to 3.0% and with an average absolute deviation of 1.2%. Figure 4 also shows that the liquid densities of methylic esters are slightly underestimated, whereas liquid densities of ethylic esters are rather overestimated. As illustrated in Figure 1, a density inversion is experimentally observed for methyl acetate and methyl propionate as well as for ethyl acetate and ethyl propionate: above 400 K, the alkyl propionate density is higher than the alkyl acetate density, whereas below this temperature it is lower. Qualitatively, such behavior is correctly predicted with our model, and quantitatively the predicted density inversion temperature (400 K) is found in excellent agreement with experiments. Saturation pressures are also found in good agreement with experimental values with an average absolute deviation of 8%. The highest relative deviations are generally obtained for the two FAMEs studied (from −12 to 20%), but it is worth mentioning that experimental data above 550 K for methyl oleate and methyl palmitate are given with large uncertainties (>15%).[65] In some rare cases, relative deviations for short alkyl-chain esters exceed 10% (methyl acetate at T_r = 0.74, ethyl acetate at T_r = 0.67, and ethyl propionate at T_r = 0.69). Finally, vaporization enthalpies are accurately predicted with an average absolute deviation of 4% and relative deviations ranging from −7 to 7%. Similarly to liquid densities, vaporization enthalpies of methylic esters are generally underestimated, whereas vaporization enthalpies of ethylic esters are overestimated. For all these saturated properties

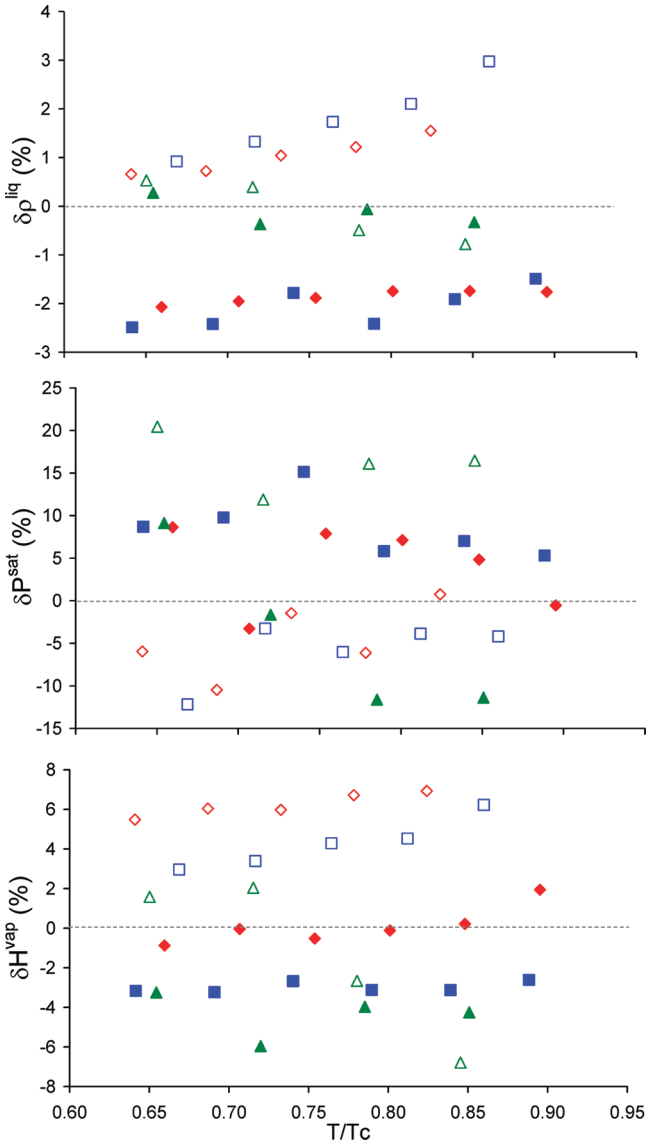

Figure 4. Relative deviations of vapor−liquid equilibrium properties between simulation data and experimental data ($\delta X = (X_{sim} - X_{exp})/X_{exp} \times 100$). blue filled box, methyl acetate; red filled diamond, methyl propionate; gree filled triangle, methyl oleate; blue open box, ethyl acetate; red open diamond, ethyl propionate; green open triangle, methyl palmitate. Top, saturated liquid density; center, vapor pressure; bottom, vaporization enthalpy.

(liquid densities, vapor pressures, vaporization enthalpies), average deviations are comparable to those already obtained for hydrocarbons and other oxygenated compounds with the AUA4 force field.[23−26,28,30,35−37]

Figure 5 shows results obtained for critical properties and normal boiling temperatures. The corresponding numerical values are given in Table 3. Again, predictions are found to be in good overall agreement with experiments. Average deviations in critical temperatures, critical densities, and normal boiling temperatures are 2.2, 2.7, and 0.7%, respectively, which is of the same order of magnitude as deviations obtained for other chemical families with this force field. Note that for methyl oleate and methyl palmitate reference data reported by the DIPPR database[39] are not from direct experiments but from predictions given by internal models. The critical density uncertainty for methyl oleate is estimated to be 25%, which can

dx.doi.org/10.1021/jp212060u | J. Phys. Chem. B 2012, 116, 3239−3248

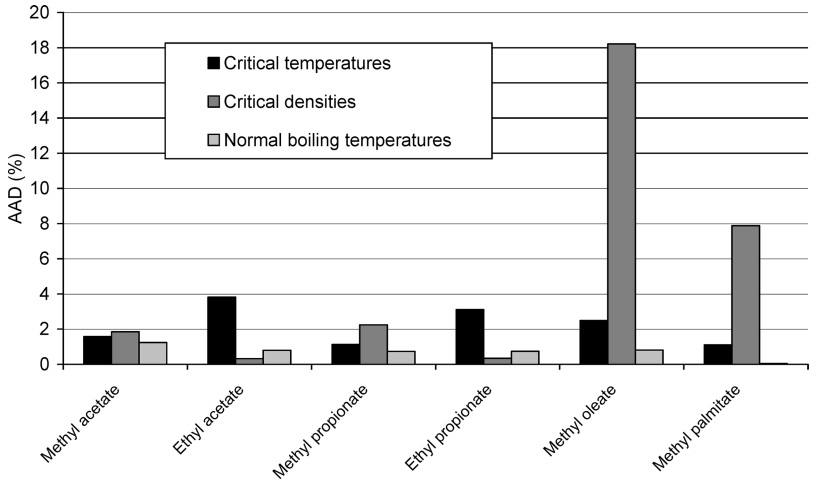

Figure 5. Absolute average deviations between reference data[39] (experiments, except for methyl oleate and methyl palmitate for which we use predicted values recommended by DIPPR) and calculated critical properties and normal boiling temperatures. AAD (%) = $\{[\mathrm{abs}(X^{calc} - X^{exp})]/X^{exp}\} \times 100$.

Table 3. Calculated Critical Temperatures, Critical Densities, and Normal Boiling Temperatures Compared to Reference Data[25] (Experiments, Except for Methyl Oleate and Methyl Palmitate for Which Reference Data Are Predicted Values Recommended by DIPPR)

	T_C (K)			ρ_C (kg/m^3)			T_b (K)		
	sim.	exp.	AAD (%)	sim.	exp.	AAD (%)	sim.	exp.	AAD (%)
methyl acetate	515	507	*1.6*	319	325	*1.8*	326	330	*1.2*
ethyl acetate	543	523	*3.8*	309	308	*0.3*	353	350	*0.8*
methyl propionate	536	530	*1.1*	305	312	*2.2*	350	353	*0.7*
ethyl propionate	563	546	*3.1*	295	296	*0.3*	375	372	*0.7*
methyl oleate	783	*764*	*2.5*	229	*280*	*18.2*	622	617	*0.8*
methyl palmitate	761	*769*	*1.1*	230	*250*	*7.9*	598	598	*0.1*

explain the high deviation (18%) observed between our simulation and this data.

4.1.3. Surface Tension. Experimental[39] and calculated liquid–vapor surface tensions for methyl acetate are shown in Figure 6 for reduced temperatures ranging from 0.7 to 0.9.

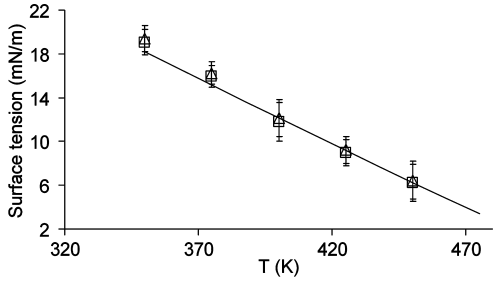

Figure 6. Surface tensions of the liquid–vapor interface of methyl acetate. Solid line, experimental data;[39] squares, calculated with the IK method; triangles, calculated with the TA method.

Numerical values are reported in Table 4. Surface tension and $p_N - p_T$ profiles along the z-axis are given in the Supporting Information (Figure S.5), as well as a snapshot of the liquid–vapor interface (Figure S.6). Results using both IK and TA methods are in good agreement with experiments since deviations are less than 4%. This result is particularly remarkable if we recall that surface tension is not a property used to parametrize this new force field, and it thus highlights its transferability.

Table 4. Experimental[39] (Smoothed) and Calculated (with IK and TA Methods) Liquid–Vapor Surface Tensions of Methyl Acetate[a]

		γ_{IK} (mN/m)		γ_{TA} (mN/m)	
T (K)	γ_{exp} (mN/m)	total	LRC	total	LRC
350	18.18	19.1_{12}	2.0	19.4_{12}	1.3
375	15.15	15.9_{10}	1.7	16.3_{10}	1.2
400	12.15	11.8_{17}	1.5	12.1_{17}	1.1
425	9.19	9.0_{12}	1.2	9.2_{12}	0.8
450	6.26	6.2_{17}	0.9	6.5_{17}	0.6

[a]The subscripts give the accuracy of the last decimal; i.e., 19.112 means 19.1 ± 1.2. The LRC columns give the contribution of the long-range correction to the total value of surface tension.

Figure 7 shows coexistence densities ρ_{liq} and ρ_{vap} determined by fitting the equilibrium density profile to a hyperbolic tangent function of the form

$$\rho(z) = \frac{1}{2}(\rho_{liq} - \rho_{vap}) - \frac{1}{2}(\rho_{liq} - \rho_{vap}) \tanh\left(\frac{2(z - z_0)}{d}\right) \quad (15)$$

where z_0 is the position of the Gibbs dividing surface and d an approximate measure of the interface thickness (adjustable parameters). An example of a density profile along the z-axis is given in the Supporting Information (Figure S.7). Figure 7 shows that saturated liquid densities calculated from

dx.doi.org/10.1021/jp212060u | J. Phys. Chem. B 2012, 116, 3239–3248

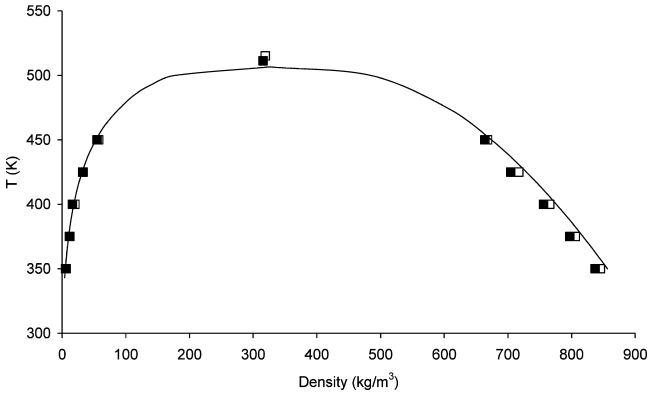

Figure 7. Methyl acetate vapor−liquid density coexistence curve. Solid line, experimental data;[39,65] filled symbols, calculated from two-phase NVT simulations; open symbols, results from Gibbs ensemble simulations.

simulations in the two-phase NVT ensemble are slightly underestimated compared to results obtained from Gibbs ensemble simulations: the average deviations between both methods are close to 1%, slightly higher than statistical uncertainties for this property (0.5%). These small deviations can be attributed to the explicit presence of the interface in the two-phase simulations. The interface further attracts the ester molecules and forms a small depletion zone in the liquid phase that may impact the density of the liquid region close to the interface. It is indeed known[47] that two-phase systems with fewer than 1000 molecules are interface dominated and that the two-phase simulations are rather designed to predict interfacial properties.

4.2. Binary Mixtures. To highlight the transferability of the force field developed here to mixtures, four binary mixtures involving esters and various oxygenated compounds are studied. The first three mixtures studied involve short alkyl-chain esters: methyl acetate + ethyl acetate at 353.15 K, methyl acetate + acetaldehyde at 373.15 K, and ethyl acetate + ethanol at 343.15 K. These mixtures are simulated to demonstrate the transferability of the force field to the prediction of pressure−composition diagrams. Acetaldehyde and ethanol are modeled with the AUA4 force field of aldehydes[36] and alcohols,[35] respectively. Figures 8−10 exhibit a good agreement between

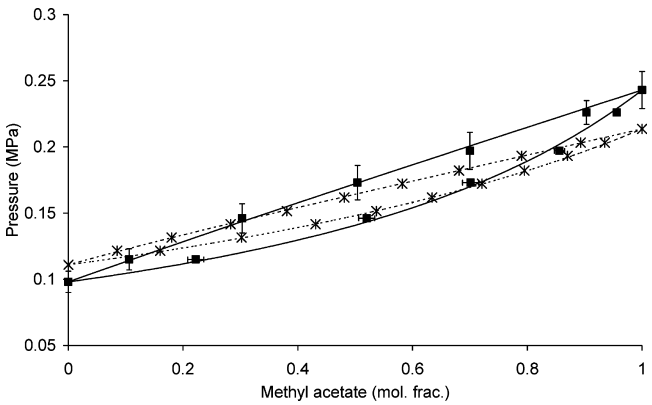

Figure 8. Pressure−composition diagram of the methyl acetate + ethyl acetate mixture at 353.15 K. Filled symbols: this work. Crosses: experimental data.[67] Lines are fits of data using the UNIQUAC activity model.

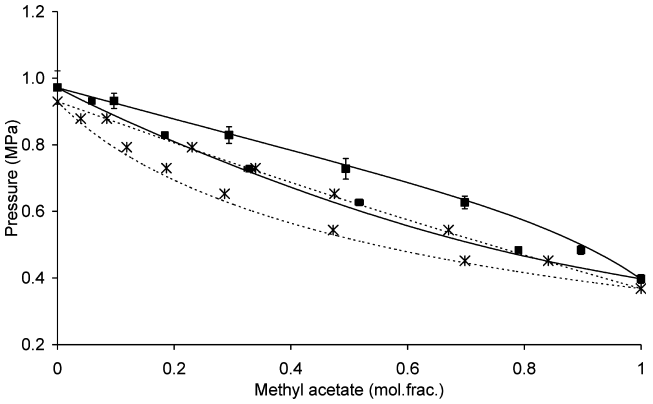

Figure 9. Pressure−composition diagram of the ethyl acetate + acetaldehyde mixture at 373.15 K. Filled symbols: this work. Crosses: experimental data.[68] Lines are fits of data using the UNIQUAC activity model.

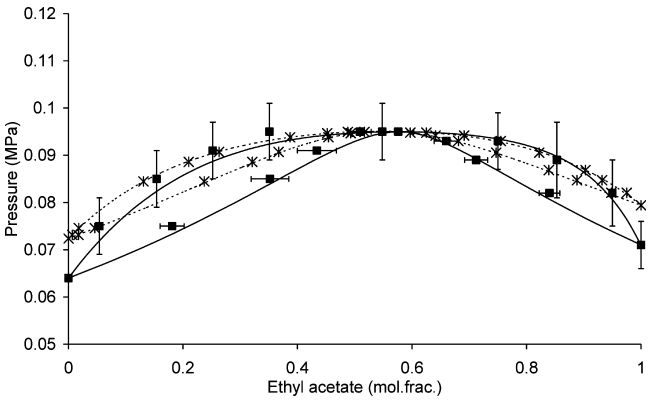

Figure 10. Pressure−composition diagram of the ethyl acetate + ethanol mixture at 343.15 K. Filled symbols: this work. Crosses: experimental data.[69] Lines are fits of data using the UNIQUAC activity model.

experimental and predicted pressure−composition diagrams. Average deviations of both bubble pressure and vapor-phase composition are about 10 and 15% for methyl acetate + ethyl acetate and methyl acetate + acetaldehyde mixtures, respectively. Since the shape and thickness of the liquid−vapor domain is accurately predicted, these deviations mainly come from deviations on pure compound vapor pressures. For the ethyl acetate + ethanol binary mixture, a positive azeotrope is experimentally observed and effectively predicted by our simulations. Deviations obtained for the vapor-phase composition and bubble pressure are about 10% and 3%, respectively. For these three mixtures, deviations between experimental and calculations are very acceptable if we recall that no empirical interaction parameters have been introduced to obtain such an accuracy. To obtain more quantitative results, an improvement would consist of proposing specific force field parameters for pure species at the temperature studied to reduce deviations in pure compound vapor pressure. However, this would reduce the transferability of the approach. For the ethyl acetate + acetaldehyde mixture, for which pure compound vapor pressures already agree quite well with experiments, the usage of binary interaction parameters would probably be required if more quantitative results are expected.

The fourth mixture studied is the methyl oleate (25 mol. %) + methanol (75 mol. %) binary system encountered in the

dx.doi.org/10.1021/jp212060u | J. Phys. Chem. B 2012, 116, 3239−3248

purification stage of biodiesel production processes. Bubble pressures are calculated at various temperatures and compared to experimental data.[66] Figure 11 exhibits a very good

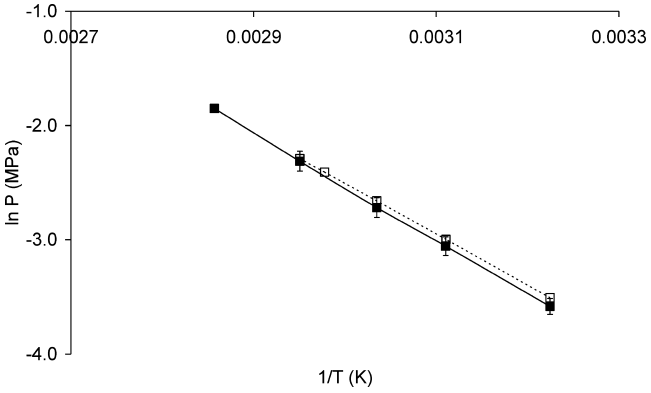

Figure 11. Bubble pressures of the methyl oleate (25 mol. %) + methanol (75 mol. %) mixture. Filled symbols, this work; open symbols,experimental data.[66] Lines are guides for the eyes.

agreement between simulation results and experiments: in the temperature range for which experimental data are available (310 to 340 K), the average deviation in bubble pressures is 5.5%. This deviation is similar to that obtained for pure methanol and pure methyl oleate vapor pressure predictions. We thus demonstrate the capability of this force field to predict properties for systems of industrial interest.

5. CONCLUSION

In this work, a new transferable united-atoms force field for carboxylate esters is proposed. All Lennard-Jones parameters of groups involved in the ester chemical function are reused from previous parametrizations of the AUA4 force field, and a unique set of partial electrostatic charges is proposed. Various short alkyl-chain esters (methyl acetate, ethyl acetate, methyl propionate, ethyl propionate) and two FAMEs (methyl oleate and methyl palmitate) are studied. Using this new force field in Monte Carlo simulations, we show that various properties of pure compounds are accurately predicted: saturated liquid densities, vapor pressures, vaporization enthalpies, critical properties, as well as liquid–vapor surface tensions. Furthermore, a good agreement is obtained for the pressure–composition diagram predictions of various binary mixtures without introducing empirical binary interaction parameters. The results obtained highlight the transferability of the proposed force field. The AUA4 force field leads to agreement with experiments similar to other united force fields such as the TraPPE-UA model. However, since it has been shown to give better predictions in pure oxygenated compound vapor pressures than other united-atoms force fields,[23,24,30,38] it offers a significant prediction improvement when simulating mixtures involving other oxygenated compounds such as alcohols. The transferability and accuracy of the AUA4 force field thus gives the opportunity to simulate mixtures of industrial interest, as shown in this work with the study of the methyl oleate + methanol mixture involved in the purification stages of biodiesel production processes.

■ ASSOCIATED CONTENT

Supporting Information

Table S.1 gives Monte Carlo moves and attempt probabilities used in Gibbs Ensemble Monte Carlo simulations. Table S.2 reports experimental and calculated saturated properties. Figure S.1 gives a molecular representation of the FAME studied. The transferability of the AUA4 force field is illustrated in Figure S.2. Figure S.3 compares experimental gas-phase dipole moments of several esters. Figure S.4 reports calculated gas-phase dipole moments. Figure S.5 gives examples of surface tension profiles for methyl acetate. Figure S.6 shows an example of a configuration of the methyl acetate liquid–vapor interface and Figure S.7 an example of a density profile. This material is available free of charge via the Internet at http://pubs.acs.org.

■ AUTHOR INFORMATION

Corresponding Author

*Tel.: +33 147526624. Fax: +33 147527025. E-mail: nicolas.ferrando@ifpen.fr.

Notes

The authors declare no competing financial interest.

■ REFERENCES

(1) Mishra, V. K.; Temelli, F.; Ooraikul, B. *J. Food. Eng.* **1994**, *23* (4), 467–480.
(2) Ling, W. H.; Jones, P. J. H. *Life Sci.* **1995**, *57* (3), 195–206.
(3) Bureau, N.; Jose, J.; Mokbel, I.; de Hemptinne, J. C. *J. Chem. Thermodyn.* **2001**, *33* (11), 1485–1498.
(4) Singh, S. P.; Singh, D. *Renewable Sustainable Energy Rev.* **2010**, *14* (1), 200–216.
(5) Leung, D. Y. C.; Wu, X.; Leung, M. K. H. *Appl. Energy* **2010**, *87* (4), 1083–1095.
(6) Jain, S.; Sharma, M. P. *Renewable Sustainable Energy Rev.* **2010**, *14* (2), 667–678.
(7) Meher, L. C.; Sagar, D. V.; Naik, S. N. *Renewable Sustainable Energy Rev.* **2006**, *10* (3), 248–268.
(8) Bloch, M.; Bournay, L.; Casanave, D.; Chodorge, J. A.; Coupard, V.; Hillion, G.; Lorne, D. *Oil Gas Sci. Tech. - Rev. IFP Energies Nouv.* **2008**, *63*, 405–417.
(9) Theodorou, D. N. *Ind. Eng. Chem. Res.* **2010**, *49*, 3047–3058.
(10) Ungerer, P.; Nieto-Draghi, C.; Lachet, V.; Wender, A.; Di Lella, A.; Boutin, A.; Rousseau, B.; Fuchs, A. H. *Mol. Simul.* **2007**, *33* (4–5), 287–304.
(11) Ungerer, P.; Tavitian, B.; Boutin, A. *Applications of Molecular Simulation in the Oil and Gas Industry*; 1st ed.; Editions Technip: 2005.
(12) Briggs, J. M.; Nguyen, T. B.; Jorgensen, W. L. *J. Phys. Chem.* **1991**, *95*, 3315–3322.
(13) Briggs, J. M.; Matsui, T.; Jorgensen, W. L. *J. Comput. Chem.* **1990**, *11* (8), 958–971.
(14) Jorgensen, W. L.; Swenson, C. J. *J. Am. Chem. Soc.* **1985**, *107* (3), 569–578.
(15) Sum, A. K.; Biddy, M. J.; de Pablo, J. J.; Tupy, M. J. *J. Phys. Chem. B* **2003**, *107* (51), 14443–14451.
(16) Nath, S. K.; Escobedo, F. A.; de Pablo, J. J. *J. Chem. Phys.* **1998**, *108* (23), 9905–9911.
(17) Kamath, G.; Robinson, J.; Potoff, J. J. *Fluid Phase Equilib.* **2006**, *240* (1), 46–55.
(18) Martin, M. G.; Siepmann, J. I. *J. Phys. Chem. B* **1998**, *102* (14), 2569–2577.
(19) Stubbs, J. M.; Potoff, J. J.; Siepmann, J. I. *J. Phys. Chem. B* **2004**, *108* (45), 17596–17605.
(20) Kamath, G.; Cao, F.; Potoff, J. J. *J. Phys. Chem. B* **2004**, *108* (37), 14130–14136.
(21) Potoff, J. J.; Siepmann, J. I. *AIChE J.* **2001**, *47* (7), 1676–1682.
(22) Maerzke, K. A.; Schultz, N. E.; Ross, R. B.; Siepmann, J. I. *J. Phys. Chem. B* **2009**, *113* (18), 6415–6425.

(23) Ungerer, P.; Beauvais, C.; Delhommelle, J.; Boutin, A.; Rousseau, B.; Fuchs, A. H. *J. Chem. Phys.* **2000**, *112* (12), 5499−5510.
(24) Bourasseau, E.; Ungerer, P.; Boutin, A.; Fuchs, A. H. *Mol. Simul.* **2002**, *28* (4), 317−336.
(25) Bourasseau, E.; Ungerer, P.; Boutin, A. *J. Phys. Chem. B* **2002**, *106* (21), 5483−5491.
(26) Bourasseau, E.; Haboudou, M.; Boutin, A.; Fuchs, A. H.; Ungerer, P. *J. Chem. Phys.* **2003**, *118* (7), 3020−3034.
(27) Contreras-Camacho, R. O.; Ungerer, P.; Boutin, A.; Mackie, A. D. *J. Phys. Chem. B* **2004**, *108* (37), 14109−14114.
(28) Bonnaud, P.; Nieto-Draghi, C.; Ungerer, P. *J. Phys. Chem. B* **2007**, *111* (14), 3730−3741.
(29) Contreras-Camacho, R. O.; Ungerer, P.; Ahunbay, M. G.; Lachet, V.; Perez-Pellitero, J.; Mackie, A. D. *J. Phys. Chem. B* **2004**, *108*, 14115−14123.
(30) Nieto-Draghi, C.; Bonnaud, P.; Ungerer, P. *J. Phys. Chem. C* **2007**, *111* (43), 15686−15699.
(31) Ahunbay, M. G.; Perez-Pellitero, J.; Contreras-Camacho, R. O.; Teuler, J. M.; Ungerer, P.; Mackie, A. D.; Lachet, V. *J. Phys. Chem. B* **2005**, *109* (7), 2970−2976.
(32) Creton, B.; de Bruin, T.; Lachet, V.; Nieto-Draghi, C. *J. Phys. Chem. B* **2010**, *114* (19), 6522−6530.
(33) Delhommelle, J.; Tschirwitz, C.; Ungerer, P.; Granucci, G.; Millie, P.; Pattou, D.; Fuchs, A. H. *J. Phys. Chem. B* **2000**, *104* (19), 4745−4753.
(34) Perez-Pellitero, J.; Ungerer, P.; Mackie, A. D. *J. Phys. Chem. B* **2007**, *111* (17), 4460−4466.
(35) Ferrando, N.; Lachet, V.; Teuler, J. M.; Boutin, A. *J. Phys. Chem. B* **2009**, *113* (17), 5985−5995.
(36) Ferrando, N.; Lachet, V.; Boutin, A. *J. Phys. Chem. B* **2010**, *114* (26), 8680−8688.
(37) Ferrando, N.; Lachet, V.; Perez-Pellitero, J.; Mackie, A. D.; Malfreyt, P.; Boutin, A. *J. Phys. Chem. B* **2011**, *115* (36), 10654−10664.
(38) Orozco, G. A.; Nieto-Draghi, C.; Mackie, A. D.; Lachet, V. *J. Phys. Chem. B* **2011**, *115* (49), 14617−14625.
(39) Rowley, R. L.; Wilding, W., V; Oscarson, J. L.; Yang, Y.; Zundel, N. A.; Daubert, T. E.; Danner, R. P. *DIPPR® Data Compilation of Pure Compounds Properties*; Design Institute for Physical Properties, AIChE: New York, NY, 2003.
(40) Merker, T.; Engin, C.; Vrabec, J.; Hasse, H. *J. Chem. Phys.* **2010**, *132* (23), 234512.
(41) Eckl, B.; Vrabec, J.; Hasse, H. *J. Phys. Chem. B* **2008**, *112* (40), 12710−12721.
(42) Eckl, B.; Vrabec, J.; Hasse, H. *Mol. Phys.* **2008**, *106* (8), 1039−1046.
(43) Jorgensen, W. L. *J. Phys. Chem.* **1986**, *90* (7), 1276−1284.
(44) Panagiotopoulos, A. Z. *Mol. Simul.* **1992**, *9* (1), 1−23.
(45) Panagiotopoulos, A. Z. *Mol. Phys.* **1987**, *61* (4), 813−826.
(46) Allen, M. P.; Tildesley, D. J. *Computer Simulation of Liquids*; Oxford University Press: New York, 1987.
(47) Frenkel, D.; Smit, B. *Understanding Molecular Simulation: From Algorithms to Applications*; Academic Press: San Diego, 1996.
(48) Mackie, A. D.; Tavitian, B.; Boutin, A.; Fuchs, A. H. *Mol. Simul.* **1997**, *19* (1), 1−15.
(49) Ungerer, P.; Boutin, A.; Fuchs, A. H. *Mol. Phys.* **1999**, *97* (4), 523−539.
(50) Ungerer, P.; Boutin, A.; Fuchs, A. H. *Mol. Phys.* **2001**, *99* (17), 1423−1434.
(51) Ferrando, N.; Defiolle, D.; Lachet, V.; Boutin, A. *Fluid Phase Equilib.* **2010**, *299* (1), 132−140.
(52) Biscay, F.; Ghoufi, A.; Lachet, V.; Malfreyt, P. *J. Chem. Phys.* **2009**, *131* (12), 124707.
(53) Trokhymchuk, A.; Alejandre, J. *J. Chem. Phys.* **1999**, *111* (18), 8510−8523.
(54) Goujon, F.; Malfreyt, P.; Simon, J. M.; Boutin, A.; Rousseau, B.; Fuchs, A. H. *J. Chem. Phys.* **2004**, *121* (24), 12559−12571.
(55) Goujon, F.; Malfreyt, P.; Boutin, A.; Fuchs, A. H. *J. Chem. Phys.* **2002**, *116* (18), 8106−8117.
(56) Ibergay, C.; Ghoufi, A.; Goujon, F.; Ungerer, P.; Boutin, A.; Rousseau, B.; Malfreyt, P. *Phys. Rev. E* **2007**, *75* (5), 051602.
(57) Orea, P.; Lopez-Lemus, J.; Alejandre, J. *J. Chem. Phys.* **2005**, *123* (11), 114702.
(58) Biscay, F.; Ghoufi, A.; Lachet, V.; Malfreyt, P. *J. Phys. Chem. B* **2009**, *113* (43), 14277−14290.
(59) Biscay, F.; Ghoufi, A.; Goujon, F.; Lachet, V.; Malfreyt, P. *J. Chem. Phys.* **2009**, *130* (18), 184710.
(60) Irving, J. H.; Kirkwood, J. G. *J. Chem. Phys.* **1950**, *18*, 817−829.
(61) Gloor, G. J.; Jackson, G.; Blas, F. J.; de Miguel, E. *J. Chem. Phys.* **2005**, *123* (13), 134703.
(62) Biscay, F.; Ghoufi, A.; Goujon, F.; Lachet, V.; Malfreyt, P. *J. Phys. Chem. B* **2008**, *112* (44), 13885−13897.
(63) Biscay, F.; Ghoufi, A.; Lachet, V.; Malfreyt, P. *Phys. Chem. Chem. Phys.* **2009**, *11* (29), 6132−6147.
(64) Biscay, F.; Ghoufi, A.; Lachet, V.; Malfreyt, P. *J. Phys. Chem. C* **2011**, *115* (17), 8670−8683.
(65) *NIST TRC Web Thermo Table* - Version 2−2011−1-Pro; NIST: Gaithersburgh, MD, 2011; http://wtt-pro.nist.gov/wtt-pro.
(66) Barreau, A.; Brunella, I.; de Hemptinne, J. C.; Coupard, V.; Canet, X.; Rivollet, F. *Ind. Eng. Chem. Res.* **2010**, *49* (12), 5800−5807.
(67) Lee, M. J.; Hsiao, C. C.; Lin, H. M. *Fluid Phase Equilib.* **1997**, *137*, 193−207.
(68) Leu, A. D.; Robinson, D. B. *J. Chem. Eng. Data* **1999**, *44*, 398−400.
(69) Mertl, I. *Collect. Czech. Chem. Commun.* **1972**, *37*, 366−374.